Short-Range Multi-Mode Continuous-Wave Radar for Vital Sign Measurement and Imaging

Avik Santra, Raghavendran Vagarappan Ulaganathan, Thomas Finke, Ashutosh Baheti,
Dennis Noppeney, Jungmaier Reinhard Wolfgang, Saverio Trotta
Infineon Technologies AG
Am Campeon 1-12, 85579 Neubiberg,
Email: avik.santra@infineon.com

***Abstract*—Short-range compact radar systems are non-invasive sensors that can locate the position and also monitor minute vibrations of the targets. They find wide use in healthcare monitoring, medical imaging, surveillance, industrial, occupancy sensing and gesture sensing applications. In this paper, we present a compact short-range 60 GHz low-power, system integrated radar system which can simultaneously operate several functional modes such as Range-Doppler Imaging, Range-Cross Range Imaging and Doppler interferometric mode without loss of performance. We also present the mechanism and processing to interleave various modes and experimentally validate the performance of the system.**

I. Introduction

Short-range localization and vital-sign tracking are two key aspects in the field of consumer electronics, medical care, surveillance, driver assistance and industrial applications ([1]-[3]). Radar can wirelessly detect the tiny physiological movements due to heartbeat and respiration activities and thus has led to applications such as sleep apnea detection, patient monitoring, presence sensing, driver monitoring and physiological monitoring in surveillance and earthquake rescue operations [7] [10] [11] [9]. Unlike other sensors, radars are non-intrusive and ubiquitous and thus do not affect the physiological body movements which arise from wearable devices. Sleep apnea detection radar [12] thus offer favorable solution, since it can accurately monitor the subjects physiological signals and body movements without affecting the sleep quality of the subject. Due to microwave penetration, in surveillance and earthquake rescue operations, radar technology can detect human activities under debris or wall even under low visibility conditions. Radars in the driver seat can be used to monitor the awake-state of the driver and used in the driver assistance system to alert the driver.

For consumer electronics, the size of the system is a key factor in order to be mounted on existing devices without affecting their functionality. Short range radar systems, featuring light weight and low cost, offer perfect solution for human presence sensing with efficient energy utilization [13]. However other sensors which detect presence based on motion, would easily fail during daily activities such as sitting, reading, or sleeping, etc. Radar sensors also find applications in tracking and classification of human activities [4], human gait classification, sudden infant death syndrome (SIDS) monitoring and elderly fall detection. Additionally several signal processing advancements have lead to tissue sensing adaptive radar (TSAR) imaging for breast cancer detection [8]. Radar sensors have also led to some emerging applications in gesture sensing [5] and object classification [6] for human-machine interaction.

The design of any radar system consists of two topics - radar hardware, including RF transceiver, waveform generator, receiver unit, antenna, and system-in-packaging, and the signal processing aspect to parse the radar return echo to extract meaningful target information. Regarding the radar hardware, continuous-wave (CW) radars have particular advantages of low transmitted power, simple structure, and high sensitivity, which makes them attractive for many of these applications. The frequency-modulated continuous-wave (FMCW) radar and the Doppler interferometric radar are two popular types of CW radars. Doppler interferometric radars can provide displacement measurement with sub-millimetric accuracy if the coherence property of the system is guaranteed. However, Doppler interferometric radars are unable to get absolute range of targets. On the other hand, the FMCW radar can obtain accurate range and Doppler related to the velocity of the target provided low Tx-Rx leakage and extremely linear ramps are ensured. In this paper, we present a short range 60 GHz multi-mode radar sensor, as depicted in Fig. 1, that can seamlessly interleave FMCW and Doppler-interferometric mode which is attractive for many of these applications.

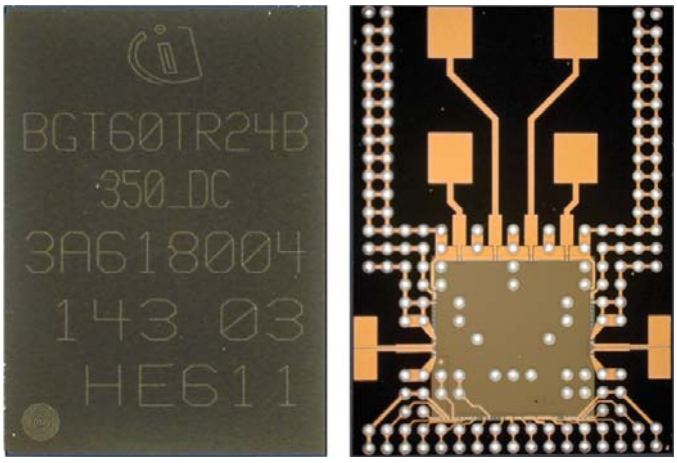

Fig. 1: Infineon's BGT60TR24B Radar Sensor

978-1-5386-4167-5/18/$31.00 ©2018 IEEE

II. FMCW, IMAGING & DOPPLER INTERFEROMETRIC RADAR

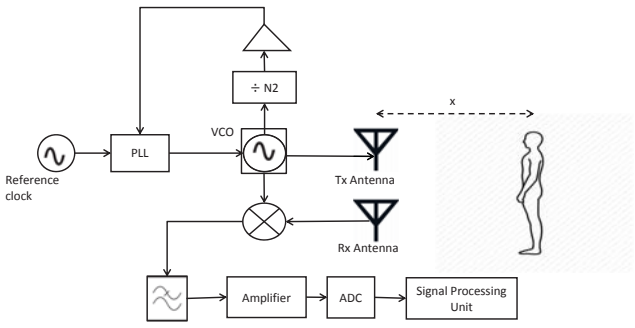

Fig. 2: RF signal chain for acquiring the digital data

FMCW radar transmits RF signal that is swept linearly in frequency over a pre-defined time. Fig. 2 depicts a block diagram of a FMCW radar which involves the use of digital synthesizers and Phased Locked Loops (PLL) for generation of a sawtooth waveform for FMCW radar, which is transmitted through the antennas to its field of view.

The frequency modulated continuous waveform is expressed as

$$s_{Tx}(t_f) = exp(j(2\pi f_c t_f + \pi\gamma t_f^2)) \quad 0 < t_f < T_c \qquad (1)$$

where f_c is the center frequency, γ is the chirp rate, i.e. B/T_c, B being the bandwidth and T_c being the chirp duration, and t_f denotes the fast time.

The received FMCW signal after being reflected from the target, x distance apart, can be expressed as

$$s_{Rx}(t_f) = \sigma exp(j(2\pi f_c(t_f - \tau) + \pi\gamma(t_f - \tau)^2)) \qquad (2)$$

where $\tau = 2x/c$ represents the propagation delay from the target and σ represents the combined effect of target RCS, propagation loss and antenna gains.

The returned echo from the target is mixed with a replica of the transmitted signal and the resulting beat signal can be measured to determine target parameters, such as position and velocity. This analog processing is referred to as 'de-ramping' or 'de-chirping' in literature. The beat signal is then low-pass filtered (LPF), which is then sampled at the analog to digital converter (ADC). The beat signal can then be expressed as

$$\begin{aligned} s_B(t_f) &= LPF\{s_{Tx}(t_f).*s_{Rx}(t_f)\} \\ &= \frac{\sigma}{2}cos((2\pi f_c\tau - 2\pi\gamma\tau^2) + 2\pi\gamma t_f 2\tau) \end{aligned} \qquad (3)$$

Thus the propagation delay is translated to beat frequency which can be identified by spectral analysis (eg. FFT). As given by eqn. (3), the range resolution is dependent on the transmit bandwidth as $c/2B$. The sampling rate required by the ADC unit is considerably lower than that required for sampling the transmit signal thus making FMCW radars compact and low cost.

A. RANGE-CROSS RANGE IMAGING

Radar Imaging is a signal processing technique to map the reflective distribution of the target from multi-frequency, multi-aspect data within the transmit beam. For a MIMO radar with $N_t = 2$ transmit (Tx) elements and $N_r = 2$ receive (Rx elements in a linear array, there are $N_t \times N_r = 4$ distinct propagation channels from the Tx array to the Rx array in a linear array configuration for azimuth angle profiling. If the transmitting source (Tx channel) of the received signals can be identified at the Rx array, a virtual phased array of $N_t \times N_r$ elements can be synthesized with $N_r + N_t$ antenna elements. A time-division multiplexed MIMO array provides a low cost solution to a fully populated antenna aperture capable of near field imaging. In Infineon's EVAL BGT60TR24B, there is a symmetrical linear arrangement of the Tx and Rx elements, with some vertical offset between the Tx array and the Rx array for reduced coupling.

Denoting the 3D positional coordinates of the Tx element as $d_i^{Tx}, i = 1, 2$ and the Rx element as $d_j^{Rx}, j = 1, 2$ in space, then on assuming far field conditions, the signal propagation from a Tx element d_i^{Tx} to a point scatterer p and subsequently the reflection from p to Rx element d_i^{Rx} can be approximated as $2 * x + d_{ij}$, where x is the base distance of the scatterer to the center of the virtual linear array, and d_{ij} refers to the position of the virtual element to the center of the array.

Assuming far field conditions are met, the time delay of radar return from a scatterer at base distance x from the center of the virtual linear array and angle θ (with respect to bore-sight) can then be expressed as

$$\tau_{ij} = \frac{2x}{c} + \frac{2d_{ij}sin(\theta)}{c} \qquad (4)$$

The transmit steering vector is expressed as

$$a_i^{Tx}(\theta) = exp(-j2\pi\frac{d_i^{Tx}sin(\theta)}{\lambda}); i = 1, 2 \qquad (5)$$

while the receiving steering vector is

$$a_j^{Rx}(\theta) = exp(-j2\pi\frac{d_j^{Rx}sin(\theta)}{\lambda}); j = 1, 2 \qquad (6)$$

where λ is the wavelength of the transmit signal. The $N_t \times N_r$ de-ramped beat signal can be stacked into a vector and the Kronecker product of the steering vector of the Tx array $a^{Tx}(\theta)$ and the steering vector of the Rx array $a^{Rx}(\theta)$, i.e. $a^{Tx}(\theta) \otimes a^{Rx}(\theta)$, can be used to resolve the relative angle of the scatterer θ. Subsequently beamforming of the MIMO array signals can be regarded as synthesizing the received signals with the Tx & Rx steering vectors. Therefore for a given range x, the azimuth imaging profile can be generated through Minimum Variance Distortionless Response (MVDR) or Capon beamforming algorithm as

$$P(\theta) = \frac{\left(a^{Tx}(\theta) \otimes a^{Rx}(\theta)\right)^H \left(a^{Tx}(\theta) \otimes a^{Rx}(\theta)\right)}{\left(a^{Tx}(\theta) \otimes a^{Rx}(\theta)\right)^H C \left(a^{Tx}(\theta) \otimes a^{Rx}(\theta)\right)} \qquad (7)$$

where $C = \mathbb{E}\{s_B(t_f = \tau)s_B(t_f = \tau)^H\}$ is the covariance of the Doppler-compensated spectrum of the baseband beat signal

at the IF frequency where target is detected, i.e. $\gamma \times 2 \times 2x/c$. whereas the cross-range resolution δR_c for the given position R is dependent on the effective aperture of the virtual array

$$\delta R_c = \frac{\lambda R}{2(N_t N_r - 1) d.cos(\theta)} \tag{8}$$

with d being the distance between the virtual antenna elements.

B. VITAL DOPPLER INTERFEROMETRY

Consider a vibrating point scatterer target, modeled for a quasi-stationary person as in Fig. 2, the distance from the radar can be expressed as

$$x(t_s) = x + \alpha_{h,max} sin(2\pi f_h t_s + \phi_h) + \alpha_{r,max} sin(2\pi f_r t_s + \phi_r) \tag{9}$$

where x is the base distance of the human to the center of the virtual linear array and t_s denotes the slow time. Human resting respiratory rate is around 12 to 20 beats/min ($f_r = 0.2 - 0.4$ Hz) with max. displacement for chest wall motion $\alpha_{r,max} = 7.5\,mm$, the heart rate can be from 50 to 200 beats/min ($f_h = 0.8 - 3.33$ Hz) with max. displacement due to heart rate $\alpha_{h,max} = 0.25\,mm$. $\phi_h \,\&\, \phi_r$ represents random phase offset from heart and respiratory vibration respectively. These band-pass filtering parameters can also be adjusted to detect the low breath and heart rates to identify vital sign abnormalities of the human.

Considering only the respiratory displacement, after low-pass filtering the base-band beat signal for the point scatterer can be expressed as

$$s(t_f, t_s) = \sigma exp\big(j(\frac{4\pi\gamma x(t_s)}{c} t_f + \frac{4\pi f_c x(t_s)}{c})\big)$$
$$= \sigma exp\big(j(\frac{4\pi\gamma x}{c} t_f + \frac{4\pi\gamma\alpha_{r,max} sin(2\pi f_r t_s + \phi_r)}{c} t_f + \frac{4\pi f_c x}{c} + \frac{4\pi f_c \alpha_{r,max} sin(2\pi f_r t_s + \phi_r)}{c})\big) \tag{10}$$

Considering $x >> \alpha_{r,max}, \alpha_{h,max}$, the second term can be ignored. Thus the frequency of the beat signal is $\frac{2\gamma x}{c}$ proportional to the base range x of the target. The change in phase over slow time, which is given by the 4^{th} term, represents the minute motion generated from the human chest wall. Similarly a corresponding term exists representing the motion due to heart movement. It is worth noting that this phase fluctuation over slow time is susceptible to human movement. The accuracy of heart/respiration estimation, which in turn is dependent on the change of phase along slow time is therefore highly sensitive to phase coherence of the radar system.

III. MULTI-MODE SHORT RANGE 60 GHz RADAR

In this section, we introduce the system parameters and the proposed methodology to operate multiple radar modes using Infineon's 60 GHz radar chipset BGT60TR24B. The chipset can generate extremely linear fast ramps from 16us to 1ms chirp time and sweep up to 7 GHz bandwidth starting from 56 GHz. In our experiments, we have set the bandwidth to 2 GHz providing 7.5 cm of range resolution and chirp time to 32 us. Linear Saw tooth ramps are generated for this bandwidth with Ns = 64 number of samples.

The chipset is provisioned to fine tune baseband amplifier gains so that it makes sure, the signal is not clipped for closer targets and also giving sufficient amplification for far-off targets. The driver enables the chipset to operate by either automatic trigger or manual trigger. In automatic trigger, the chipset is programmed with the required chirp parameters with constant time between the chirps. Back-scattered signals with this constant time interval are stored in the on-chip memory and through protocol communication transmitted to Application Processor or Host for processing. With manual trigger, accurate target bin estimation can be performed, wherein every chirp is triggered and beat signal is extracted manually on demand. For maintaining the time coherency requirements of both the imaging and vital sensing modes, we operate the radar sensor in automatic trigger.

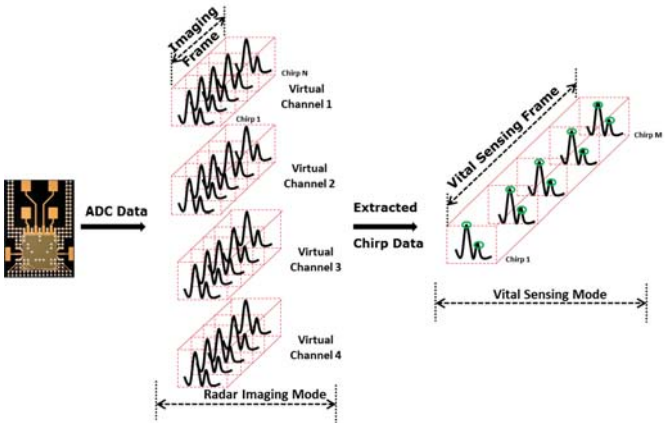

Fig. 3: Multi-mode processing for Radar Imaging and Vital sensing

Fig. 3 represents how the different operation modes, such as Range-Cross Range imaging and vital signal monitoring, are interleaved across different frames. For the radar Range-Cross Range imaging, N (for e.g. N = 16) consecutive chirps from the radar physical frame across all the virtual channels are extracted and processed using the MVDR beamforming algorithm as explained in Section II A. For imaging mode, an initial range detection is performed through adaptive thresholding, an FFT is computed over the slow-time for Doppler estimation. We use the detected Doppler bins in Eq. (7) for computing the cross-range spectrum for all detected range bins (down-range). For vital sign measurement, chirps spaced 20 ms apart are extracted from across the radar physical frame and accumulated for M = 512 chirps, providing us the vital-sensing frame. The Range-Cross Range imaging is generated every 320 ms whereas the vital signal detection/estimation is computed every 10 sec. However the update rate of the vital sign computation can be increased by sliding window approach, if desired. The initial range detection performed in Range-Cross Range imaging mode is passed to the vital sign monitoring mode as potential targets.

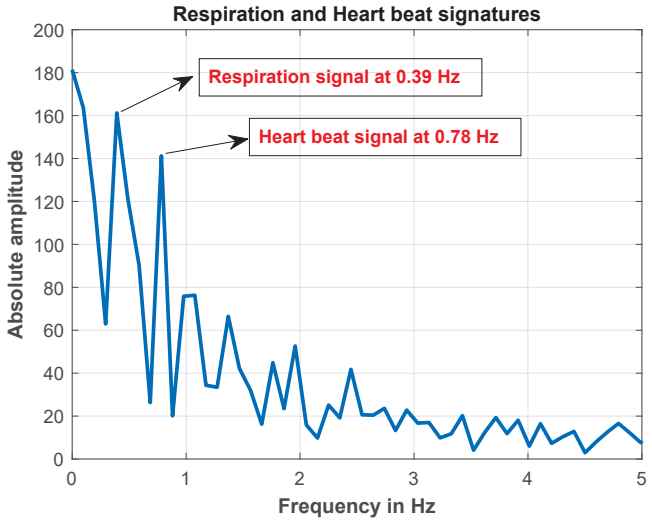

Fig. 4: Extracted Respiratory and Heart-beat Signal

For vital signal detection, since the respiration and heart signals exist simultaneously, the phase modulation inevitably brings in harmonics and inter-modulation components between respiration and heart signal which are not desirable. These interfering signals may hide or confuse the detection of heartbeats. To circumvent the issue of intermodulation components, we have two different bandpass filter for heart signal estimation, $f_{c1} = 1.4$ Hz and $BW_1 = 1.2$ Hz for normal resting heart and $f_{c1} = 2.5$ Hz and $BW_1 = 1.2$ Hz for exercised heart. For respiratory signal extraction an IIR filter with center frequency $f_{c2} = 0.3$ Hz and bandwidth $BW_2 = 0.2$ Hz is used. However, it is worth mentioning that these heart signal filters would still have issues with lower and higher true heart beat respectively of the filter band. Fig. 4 depicts the low frequency spectral peaks corresponding to the respiration and heart beat signature from a human sitting in front of the sensor.

In Fig. 5, we explain the signal processing pipeline to extract the vital signal for estimation and tracking. The potential range gates are chosen through adaptive threshold criteria determined in the Range-Cross Range imaging mode and then the corresponding range bin's phase is extracted and passed through heart and breathing bandpass IIR filters. A vital-Doppler detection over the vital frequency band is performed to eliminate false static target bins. If the vital signal is detected in the range bin, the signal is smoothened followed by respiration/heart beat calculation through spectral estimation techniques. To make the heart signal estimation robust to intermodulation and interference, we process the heart/respiratory beats through median filtering followed by $\alpha\beta$ tracking algorithm to stabilize from intermittent movements.

IV. EXPERIMENTAL RESULTS & DISCUSSION

In this section, we present the experimental setup and discuss the results. Fig. 6 and Fig. 7 presents the experimental scene and the corresponding Range-Cross Range image respectively, wherein a chair and the person is sitting 0.7 m away from the radar sensor but at different cross range. Fig. 8 and Fig. 9 depicts another experimental scene and its corresponding Range-Cross Range image, wherein two persons are sitting in front of the sensor but at different down-range bins 0.7 m and 1.7 m respectively.

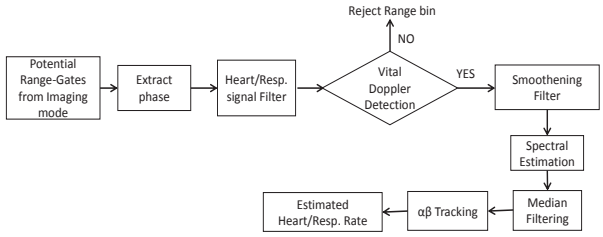

Fig. 5: Heart Rate Extraction Algorithm

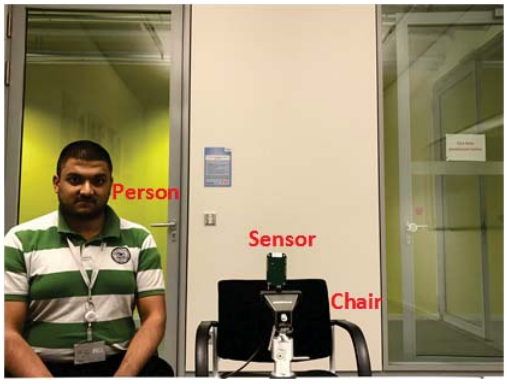

Fig. 6: Setup with two targets at same down-range bin

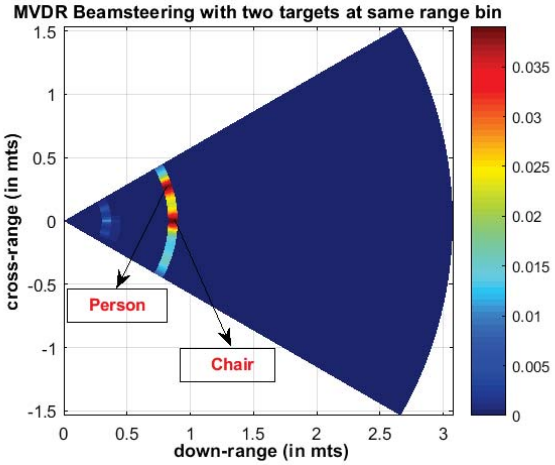

Fig. 7: MVDR Range Cross-Range plot

The threshold in case of indoor environment is set such that the maximum detectable range is 4 m, thus the door which is at 5.2 m from the sensor is not visible in the image.

Fig. 8: Setup with two targets at different range bins

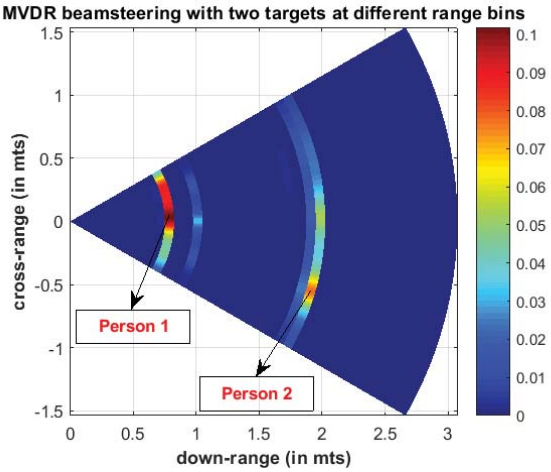

Fig. 9: MVDR Range Cross-Range plot

The heart-rate extraction results are cross-referenced with the results from a standard pulsoximeter and it yields that the sensor can achieve an accuracy of $\pm$ 2 heart bpm within 20 sec of settling time in case of a single person. However, it must be noted that for people with extremely low heart beats ($<$ 60 bpm), the algorithm picks the inter-modulation component resulting in estimation errors. Theoretically, the radar sensor can detect $R_{max}/\delta R$ vital signatures in its field of view, where R_{max} is the maximum detectable range and δR is the radar range resolution. However practically this is limited by the spectral leakage into neighboring range bins caused by the periodic vital displacement at a given range bin. The spectral leakage also results in vital sign estimation errors in case of multiple persons in the field of view. This undesired phenomenon can be mitigated to some extent through careful choice of window function.

V. Conclusion

This paper presents a compact low cost, low power, system integrated short range 60 GHz radar. It is demonstrated here how the sensor can be used seamlessly in both imaging mode to localize targets in its field of view and vital Doppler interferometric mode to discriminate between static objects and multiple humans. The same radar system can also be used to adaptively interleave ISAR imaging and gesture sensing modes along with imaging and Doppler interferometric mode and is the focus of our future research.

References

[1] Peng, Zhengyu and Muñoz-Ferreras, José María and Tang, Yao and Liu, Chenhui and Gómez-García, Roberto and Ran, Lixin and Li, Changzhi, "A portable FMCW interferometry radar with programmable low-IF architecture for localization, ISAR imaging, and vital sign tracking", in *IEEE Transactions on Microwave Theory and Techniques*, vol. 65, no. 4, pp. 1334–1344, 2017.

[2] Li, Changzhi and Peng, Zhengyu and Huang, Tien-Yu and Fan, Tenglong and Wang, Fu-Kang and Horng, Tzyy-Sheng and Muñoz-Ferreras, José-María and Gómez-García, Roberto and Ran, Lixin and Lin, Jenshan, "A Review on Recent Progress of Portable Short-Range Noncontact Microwave Radar Systems", in *IEEE Transactions on Microwave Theory and Techniques*, vol. 65, no. 5, pp. 1692–1706, 2017.

[3] Peng, Zhengyu, and Changzhi Li. "A 24-GHz portable FMCW radar with continuous beam steering phased array (Conference Presentation)", Radar Sensor Technology XXI . Vol. 10188. International Society for Optics and Photonics, 2017.

[4] Kim, Youngwook, and Hao Ling. "Human activity classification based on micro-Doppler signatures using a support vector machine." IEEE Transactions on Geoscience and Remote Sensing, vol. 47, no. 5, pp. 1328-1337, 2009.

[5] Lien, Jaime, Nicholas Gillian, M. Emre Karagozler, Patrick Amihood, Carsten Schwesig, Erik Olson, Hakim Raja, and Ivan Poupyrev. "Soli: Ubiquitous gesture sensing with millimeter wave radar." ACM Transactions on Graphics (TOG) vol. 35, no. 4, pp. 142, 2016.

[6] Yeo, Hui-Shyong, Gergely Flamich, Patrick Schrempf, David Harris-Birtill, and Aaron Quigley. "Radarcat: Radar categorization for input & interaction." In Proceedings of the 29th Annual Symposium on User Interface Software and Technology, pp. 833-841, ACM, 2016.

[7] Li, Changzhi, Victor M. Lubecke, Olga Boric-Lubecke, and Jenshan Lin. "A review on recent advances in Doppler radar sensors for noncontact healthcare monitoring." IEEE Transactions on microwave theory and techniques, vol. 61, no. 5, pp. 2046-2060, 2013.

[8] Fear, Elise C., J. Bourqui, C. Curtis, D. Mew, B. Docktor, and C. Romano. "Microwave breast imaging with a monostatic radar-based system: A study of application to patients." IEEE transactions on microwave theory and techniques, vol. 61, no. 5, pp. 2119-2128, 2013.

[9] Gu, Changzhan. "Short-range noncontact sensors for healthcare and other emerging applications: A review." Sensors vol. 16, no. 8 (2016): 1169.

[10] Gu, Changzhan, and Changzhi Li. "From tumor targeting to speech monitoring: Accurate respiratory monitoring using medical continuous-wave radar sensors." IEEE Microwave Magazine, vol. 15, no. 4, pp. 66-76, 2014.

[11] van Loon, K., M. J. M. Breteler, L. van Wolfwinkel, AT Rheineck Leyssius, S. Kossen, C. J. Kalkman, B. van Zaane, and L. M. Peelen. "Wireless non-invasive continuous respiratory monitoring with FMCW radar: a clinical validation study." Journal of clinical monitoring and computing, vol. 30, no. 6, pp. 797-805, 2016.

[12] Li, Changzhi, Jenshan Lin, and Yanming Xiao. "Robust overnight monitoring of human vital signs by a non-contact respiration and heartbeat detector." In Engineering in Medicine and Biology Society, 2006. EMBS'06. 28th Annual International Conference of the IEEE, pp. 2235-2238. IEEE, 2006.

[13] Yavari, Ehsan, Chenyan Song, Victor Lubecke, and Olga Boric-Lubecke. "Is there anybody in there?: Intelligent radar occupancy sensors." IEEE Microwave Magazine, vol. 15, no. 2, pp. 57-64, 2014.